Quantification of the Effects of Using Slats on the Inner Part of a 10MW Rotor

Gaunaa, Mac; Zahle, Frederik; Sørensen, Niels N.; Bak, Christian

Published in:
Proceedings of EWEA 2012 - European Wind Energy Conference & Exhibition

Publication date:
2012

Document Version
Publisher's PDF, also known as Version of record

Quantification of the Effects of Using Slats on the Inner Part of a 10MW Rotor

Mac Gaunaa, Frederik Zahle, Niels N. Sørensen, Christian Bak
Wind Energy Department, DTU, DK-4000 Roskilde, Denmark
macg@dtu.dk

Abstract

The present work attempts at quantifying the effects of using slats on the inner part of a modern multi-MW rotor as a post-fix to increase power production. In the process of doing this, the main behavior of the underlying physics is illuminated using a simplified BEM approach, and the effect of the lift and drag forces on local and integral power production and thrust is shown in a clear way. Two different methods (a BEM based and a free wake lifting line method) for determining angles of attack and lift coefficients corresponding to a specific loading on the inner part of the rotor are shown, and the results are compared. For the design of the slats, a 2D CFD based optimization approach is shown, and the final results from the algorithm for four specific inner airfoil sections on the multi-MW rotor is shown. Finally, the impact of the alteration of the airfoil section force characteristics are shown in the design point using both a BEM based and a free wake lifting line method, and BEM based results are used to asses the effects of the addition of the slats on the annual energy production.

1 Introduction

Recent aerodynamic investigations [1] have shown that the rotational effects neglected in the standard Blade Element Momentum (BEM) theory cause a less than optimal power production due to a too low loading on the inner part of the rotor if the rotor is designed using standard BEM theory. The additional loading needed should counterbalance the increased pressure jump over the rotor disc due to the rotation of the wake after the rotor. Since most tools for rotor design are based on the standard BEM formulation, a rotor designed for maximum energy yield with these tools will be too lightly loaded toward the rotor center. Apart from this, the combination of material cost, stand still loads and maximum chordlength due to transportation requirements have resulted in the inner part of conventionally designed MW-size wind turbine rotors being loaded significantly less than what is required for optimal power production. A quantification of the obtainable additional maximum power production can be seen in the work by Johansen et.al. [2], where CFD computations on a rotor designed for maximum power production is compared to the IEA/NREL/Upwind 5MW Reference Wind Turbine (RWT5). This study showed that an increase in C_P of 8% is obtainable at the cost of a 12% increase in C_T if the loading on the inner part of the rotor is increased. As done in [2] this can be accomplished by increasing the chordlength of the rotor. However, issues linked to transportation, extreme loads and cost renders that type of design uninteresting for the wind industry. Recent investigations, however, have indicated that the use of multiple element airfoils on the inner part of the rotor, where the main airfoil sections have a high relative thickness due to the structural constraints, may be able to increase the lift coefficient, and hence loading, enough to obtain a significant increase in power production without increasing the chordlength of the blade [3, 4]. Due to the relatively low maximum C_P of the 5MW reference turbine, caused by the very low loading toward the root of the blade, investigations aimed at estimating a representative increase in the power production potential may overestimate the potential of lift/power enhancement methods when determining the potential on this turbine. For this reason, the present work will be based on the first design iteration of the ongoing design of a 10MW reference wind turbine (RWT10), from the Danish LightRotor project [5], which is believed to have a design strategy closer to the present day multi MW wind turbine rotors. This way, the conclusions obtained here will be more interesting in terms of estimating the benefits of using multiple element airfoils on commercial turbines. In order to simplify matters we are in this work investigating only the potential of fitting

the slats on a previously designed rotor. This way the design problem is simplified because fewer degrees of freedom is involved. On the other hand, the beneficial effect of using slats on the inner sections of wind turbine rotors may be greater if both the main rotor and the slats are designed simultaneously because the main airfoil may have an angle of attack where it is hard to make the slatted combination perform well, which can be avoided if during the design process it is allowed to retwist (and possibly also modify the chordlength) the main wing. Prior to digging into the actual slat design and analysis of the obtainable gains, the different computational tools needed for the process will be described, along with a simplified version of the BEM equations for simple initial design and analysis of the inner sections of wind turbines.

2 Aerodynamic Computational Tools

In this section the computational tools used for the rotor and airfoil computations are described briefly. Please consult the references for a more thorough description.

2.1 Rotor aerodynamics: BEM

The BEM method used in the present study correspond to the steady basic part of what is in the aeroelastic code HAWCII [6]. It should be noted that the corrections for extra thrust and power due to wake rotation and lower loading toward the tips due to radial flow as described by Madsen and coworkers in [1] is not included in either HAWCII or in the BEM code used for the present results.

2.2 Rotor aerodynamics: Free Wake Lifting Line

For the free wake lifting line results in the present work the code by Gaunaa was used. The method is based on a free wake lifting line method, where steady state operation is used to speed up the convergence of the solution by use of a non-parabolic solution technique and use of symmetry in the wake. For configurations with non-straight wings the contributions from the bound vorticity on the total relative velocity is modelled using a vortex-lattice type method. Forces due to drag are added in the relative flow direction using the inviscid force magnitude combined with the lift to drag ratios. The method can be run with either a given circulation distribution or the circulation distribution can be obtained iteratively from the rotor geometry combined with 2D aerodynamic force coefficients and the lifting line method. Please refer to [7–9] for the details of the method.

2.3 2D airfoil aerodynamics: EllipSys2D

The 2D airfoil aerodynamics used in the present work, including those in the optimization algorithm, are obtained using the 2D version of DTU's in-house incompressible CFD solver EllipSys. The EllipSys2D code is a multiblock finite volume discretization of the incompressible Reynolds-averaged Navier-Stokes (RANS) equations in general curvilinear co-ordinates. In the present work the turbulence in the boundary layer is modelled by the $k-\omega$ SST model, and all computations are performed using a fRe Laminar-turbulent transition model. The mesh generation is done with hypgrid [10] an in-house hyperbolic mesh generation code. A general description of the EllipSys code is given in [11–13]. A general validation for the capability with multiple element airfoils can be found in [14], and applications to the case of multiple element cases with a thick main airfoil can be found in [3, 4, 15, 16].

3 2D Optimization Method

The optimization method developed for this work was programmed in Python using the open-source Multidisciplinary Design Analysis and Optimization framework OpenMDAO [17] for connecting the different components in the optimization. The optimization framework consisted of four main components:

1. A component class for manipulation of an airfoil geometry,
2. An ExternalCode class that automates mesh generation,
3. An ExternalCode class for executing CFD simulations,
4. A Driver class that wraps the HAWTOPT optimizer.

The OpenMDAO framework thus handles the exchange of design variables between the airfoil geometry manipulation class and the optimizer, setup of design variable bounds, constraints and evaluation of the objective function, see Figure 2. The parallel EllipSys2D CFD simulations were run sequentially on a computing cluster on 19 CPUs.

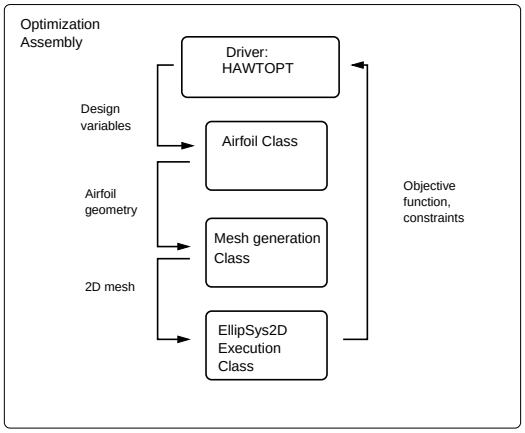

Figure 1: Geometrical parameters that the optimization code can adjust to meet the optimization targets.

The overall goal of the optimization is to achieve a slat configuration which meets the target lift coefficients at an angle of attack which can be either specified or unspecified, while also providing a high maximum lift beyond the design point to provide enough lift reserve to tackle large changes in angle of attack.

The optimizer attempts to minimize a function which is composed of two factors: $C_{l,target}$, at the specified target angle of attack, α_{target}; the function A_1 which evaluates the lift-to-drag ratio at the target angle of attack; and the function A_2, which seeks to maximize the lift coefficient at an angle of attack 5 degrees higher than α_{target}.

The two functions A_1 and A_2 are normalized with a predefined reference lift-to-drag ratio and lift coefficient.

$$CostFun = -\left(A_1 + A_2\right) \tag{1}$$

with the two functions A_1 and A_2 is defined as

$$A_1 = \frac{C_l(\alpha_{target})}{C_d(\alpha_{target})} \cdot \frac{1}{(C_l/C_d)_{target,ref}} \cdot K_{optim} \tag{2}$$

$$A_2 = \frac{C_l(\alpha)}{C_{l,maxref}} \cdot (1 - K_{optim}) \tag{3}$$

K_{optim} is a factor in the range [0:1] which biases the cost function towards obtaining the target lift coefficient or lift-to-drag ratio. Although the lift-to-drag ratio is typically not as important towards the root section of a blade as it is further out on the blade, it is needed in this optimization method in order to force the optimization towards slat configurations where the flow is attached.

For each optimization iteration two evaluations are thus needed: one at the target angle of attack, α_{target}, and another at α_{target}+5 degrees. Besides the angle of attack, the optimization code was allowed to vary the following geometrical parameters of the slat:

- Position of slat trailing edge measured as:
  - Surface distance along main airfoil surface from leading edge,
  - Normal distance from main airfoil surface to slat trailing edge.
- Slat angle relative to main airfoil.
- Slat camber (parabolic curve).

Figure 2 shows a schematic drawing of an airfoil fitted with a slat with the optimization parameters indicated.

4 Approximate Aerodynamics from BEM Theory

In order to gain the necessary insight into the key elements of the physics at play, an approximate model for the aerodynamics, based on BEM theory, will be here. In this model, the effects that lift to drag ratio, radial location, local thrust coefficient and tip speed ratio have on the power production are described in a simple way. Also the approximate model can be used to obtain a good starting guess for the design of the slatted rotor. Since the focus of this study lies far from the tip on the rotor, tip effects will not be included in the present approximate analysis. Furthermore, it is the authors' opinion that the root corrections used in some BEM based codes, which is usually a modified tip-correction applied to the root section of the blades, are not really motivated by any stringent analysis of the physics of the problem. This probably also the reason why many aeroelastic simulation codes such as Flex5 and HAWCII does not include root corrections. Therefore, a root correction is not included in the approximate analysis shown here either.

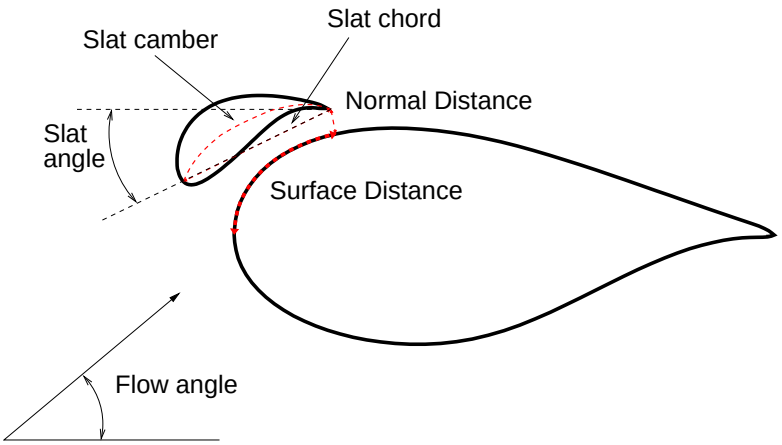

Figure 2: Geometrical parameters that the optimization code can adjust to meet the optimization targets.

4.1 Definitions & Basics

The non-dimensional quantities used in the present analysis are defined below. The integral power and thrust coefficients are defined as

$$C_P = \frac{P}{0.5\rho A V_\infty^3} \quad (4)$$

$$C_T = \frac{T}{0.5\rho A V_\infty^2} \quad (5)$$

From these, the corresponding local quantities are defined as

$$C_{p,loc} = \frac{dP}{0.5\rho V_\infty^3 dA} = \frac{dP/dr}{\pi\rho V_\infty^3 \tilde{r} R} \quad (6)$$

$$C_{t,loc} = \frac{dT}{0.5\rho V_\infty^2 dA} = \frac{dT/dr}{\pi\rho V_\infty^2 \tilde{r} R} \quad (7)$$

In the expressions above, the non-dimensional local radial position is

$$\tilde{r} = \frac{r}{R} \quad (8)$$

From the equations above it is seen that the relation between local and integral rotor quantities are

$$C_P = \int_0^1 2\tilde{r} C_{p,loc} d\tilde{r} \quad (9)$$

$$C_T = \int_0^1 2\tilde{r} C_{t,loc} d\tilde{r} \quad (10)$$

The axial induction factor is defined as the fraction the free stream flow is decreased when it reaches the rotor disc. Therefore the axial speed relative to the rotor can be written as

$$V_{axial} = V_\infty (1 - a) \quad (11)$$

Similarly, the induction in the tangential direction at the rotor disc can be denoted with the axial induction factor, a', which gives the tangential induction (positive in the direction opposite to the rotor rotation) as a fraction of the relative eigen-speed of the blade section due to the rotors rotation

$$V_{tang,induced} = \Omega r a' \quad (12)$$

Therefore the tangential velocity component relative to the blade sections on the blade can be written as

$$V_{tang} = \Omega r (1 + a') = V_\infty \lambda \tilde{r} (1 + a') \quad (13)$$

Tip speed ratio is defined as

$$\lambda = \frac{\Omega R}{V_\infty} \quad (14)$$

and lift, drag and normal force coefficients are defined as

$$C_l = \frac{l}{0.5\rho c V_{rel}^2} \quad (15)$$

$$C_d = \frac{d}{0.5\rho c V_{rel}^2} \quad (16)$$

$$C_y = \frac{F_y}{0.5\rho c V_{rel}^2} \quad (17)$$

where the relative velocity can be determined from Pythagoras' relation

$$V_{rel}^2 = V_{axial}^2 + V_{tang}^2$$

$$\Leftrightarrow \left(\frac{V_{rel}}{V_\infty}\right)^2 = (1 - a)^2 + (\lambda\tilde{r})^2 (1 + a')^2 \quad (18)$$

4.2 Analysis and initial design algorithm

We start out with the relation between axial induction and local thrust coefficient used in HAWCII [6].

$$a = k_3 C_{t,loc}^3 + k_2 C_{t,loc}^2 + k_1 C_{t,loc} \quad (19)$$

where the coefficients in the expression

$$\begin{aligned} k_1 &= 0.25116 \\ k_2 &= 0.05450 \\ k_3 &= 0.08921 \end{aligned}$$

are determined such that the relation between a and $C_{t,loc}$ are very close to 1D classic momentum theory for $a < 1/3$ and close to the usually adopted corrections for high loading. From this expression the axial induction factor corresponding to a given local thrust coefficient can be determined.

The flow angle relative to the rotor is

$$\phi = \arctan\left(\frac{V_{axial}}{V_{tang}}\right) = \arctan\left(\frac{1}{\tilde{r}\lambda}\frac{1-a}{1+a'}\right) \quad (20)$$

The relation between the forces normal to the rotor-plane and the lift and drag values result in the following relation between the corresponding non-dimensional quantities

$$\begin{aligned} C_y &= C_l\cos(\phi) + C_d\sin(\phi) \\ &= C_l\left(\cos(\phi) + \frac{1}{\left(\frac{C_l}{C_d}\right)}\sin(\phi)\right) \end{aligned} \quad (21)$$

It is usually a very good assumption to neglect the drag forces when computing the normal forces[1] [18]

$$\frac{dT}{dr} \simeq N_B l\cos(\phi) \quad (22)$$

This is not the case for the tangential forces, which relates to the power production, so in this case we have

$$\frac{dP}{dr} = N_B r\Omega l\left(\sin(\phi) - \frac{1}{\left(\frac{C_l}{C_d}\right)}\cos(\phi)\right) \quad (23)$$

[1] After the approximate solution is obtained, the validity of this assumption can be checked, since the assumption corresponds to $\mid (C_l/C_d)/tan(\phi) \mid \gg 1$, which for the case investigated here is fulfilled as long as $C_l/C_d \gg 1$.

Combining Equations 22 and 23 with Equations 6 and 7 we therefore get after some reduction (using Equations 8, 14 and 20), that

$$\begin{aligned} \frac{C_{p,loc}}{C_{t,loc}} &\simeq \tilde{r}\lambda\left(\frac{V_{axial}}{V_{tang}} - \frac{1}{\left(\frac{C_l}{C_d}\right)}\right) \\ &= \frac{1-a}{1+a'} - \frac{\tilde{r}\lambda}{\left(\frac{C_l}{C_d}\right)} \end{aligned} \quad (24)$$

At this point the last thing we need to be able to determine to know the approximate flow behavior at the rotor disc is the tangential induction. For this, the tangential momentum equation is employed[2], see for instance Hansen [19]. The result in terms of the local power coefficient is

$$C_{p,loc} = \lambda^2\tilde{r}^2 4a'(1-a) \quad (25)$$

If we now combine this way of determining $C_{p,loc}$ with the approximate one in Equation 24, we can determine the tangential induction factor. The solution for $\lambda\tilde{r} < (1-a)C_l/C_d$ and $\mid C_l/C_d \mid \gg 1$, the solution is

$$a' = \frac{1}{2}\sqrt{1 + \frac{C_{t,loc}}{\lambda^2\tilde{r}^2}} - \frac{1}{2} \quad (26)$$

Before we proceed to determining angles of attack and lift coefficients needed, we want to point out some observations that may be drawn from Equations 24 and 9 regarding the nature of the individual contributions to the integral power coefficient.

$$C_P \simeq C_{P,inviscid} + C_{P,drag} \quad (27)$$

where

$$C_{P,invisc} = \int_0^1 2C_{t,loc}\frac{1-a}{1+a'}\tilde{r}d\tilde{r} \quad (28)$$

$$C_{P,drag} = -\int_0^1 2C_{t,loc}\frac{\lambda\tilde{r}^2}{\left(\frac{C_l}{C_d}\right)}d\tilde{r} \quad (29)$$

It is seen that the total power coefficient consists of a sum of an inviscid part, $C_{P,invisc}$, and a drag penalty part, $C_{P,drag}$. It is noted that for the inviscid term in the case of constant loading and $a' \simeq 0$ (corresponding to a high tip speed ratio) we get the classical 1D momentum result: $C_{P,invisc} = C_T(1-a)$. As a' increases, this value decreases. Several papers have been written on the effect of the term

[2] where the tangential velocity in the non-rotating coordinate system is 0 before the rotor and $2\Omega r a' = 2V_\infty\lambda\tilde{r}a'$ after the rotor

not included in this classical way of analyzing things, the pressure drop due to the rotation of the wake, which results in an addition to the thrust force, and also a slight increase to the available power. This will, however, not be included in this analysis because what we are after is an approximate analysis. The other part of the power coefficient, $C_{P,drag}$, due to less than infinite lift-to-drag ratios is always negative. Drag always reduce the power output. What is interesting is that Equation 29 show how big the drag penalty is. It is seen that the 'badness' of non-infinite lift-to-drag scales linearly with the tip speed ratio and inversely with C_l/C_d. Also interesting is the observation that the term $\tilde{r}^2$ is also in the integrand. From this we see just how much less important having a high lift-to-drag ratio on the inner part of the rotor compared to the outer part is: for instance 25 times more important at $\tilde{r} = 0.75$ than at $\tilde{r} = 0.15$ for the same drag power loss per rotor span length. Here one may argue that the 'badness' of the drag should be compared to the equivalent magnitude of the 'goodness' that the lift/thrust part generates, which scale linearly with radius. In this case we see that for constant a and a' the drag loss scale with the factor $\lambda\tilde{r}/(C_l/Cd)$ relative to the productive term. This means that drag loss increase linearly with radius relative to the 'clean' thrust production term, so in this case drag could be said to be 5 times more important at $\tilde{r} = 0.75$ than at $\tilde{r} = 0.15$.

Now that the flow angles, ϕ, are known from Equation 20 it is easy to determine the angles of attack at the given rotor loading situation from simple geometry if the blade twist, γ_{twist}, and pitch, θ_{pitch}, are known

$$\alpha = \phi - \gamma_{twist} - \theta_{pitch} \tag{30}$$

The relations effectively used here to determine the angle of attack simply assumes that the induced velocity stems from interaction with only the lift force, so the drag part of the total force is omitted. Usually, estimation of flow angles using only the lifting part of the total forces is a good approximation [18], and is common practice in for instance the BEM based aeroelastic code Flex5.

In order to determine the C_l corresponding to the local thrust and flow velocities at the disc we simply note that

$$\frac{dT}{dr} = F_y N_B \tag{31}$$

and use this with Equations 17, 21, 7 and the definition of the non-dimensional radial position, $\tilde{r}$, in Equation 8 to arrive at

$$C_l = \frac{C_{t,loc} 2\pi\tilde{r}}{\frac{c}{R} N_B \left(\frac{V_{rel}}{V_\infty}\right)^2 \left(\cos(\phi) + \frac{1}{\left(\frac{C_l}{C_d}\right)} \sin(\phi)\right)} \tag{32}$$

where the squared velocity ratio and the flow angles are known from Equations 18 and 20.

Now we have the means to compute all important information needed from the approximate solution. The needed steps are outlined in the list below

1. Set desired target local thrust coefficient, $C_{t,loc}$, along the (inner part of the) rotor. Values close to $C_{t,loc} = 8/9$ yield maximum power.
2. Determine the corresponding axial induction coefficient from Equation 19.
3. Determine the corresponding approximate tangential induction coefficient from Equation 26.
4. Angle of attack (based on main airfoil section direction), α_{target}, from Equation 30
5. Lift coefficient (based on main airfoil section chordlength), $C_{l,target}$, from Equation 32
6. Optional determination of different interesting local and integral loading quantities

   $C_{p,loc}$**:** Local power coefficient from Equation 24

   $C_{P,invisc}$**:** Integral inviscid component of C_P, Equation 28

   $C_{P,drag}$**:** Integral drag penalty component of C_P, Equation 29

   C_P**:** Integral power coefficient, Equation 27 or 9

Please note that it is relatively straightforward also to modify an existing BEM code to obtain this type of results without the approximations. The outlined expressions are just simpler, require no numerical iteration, and the analytical expressions facilitate a better understanding of the key elements of the physical problem at hand. Furthermore, as will be outlined by the differences between free wake and BEM code results, the approximations made in standard BEM codes and the general physics of the problem already results in a quite large uncertainty as the rotor axis is approached.

5 Results and Discussion

In this section results from the previously explained models will be shown and discussed.

1. The validity of the initial design algorithm will be assessed using the free wake algorithm.

2. Four different 2D sections from the innermost part of the rotor will get optimized slats using the 2D slat optimization tool.

3. The power production increase will be evaluated using both the power coefficient in the design point and the annual energy production.

5.1 Evaluation of validity of the initial design algorithm & Design targets for 2D optimization

In order to check how well the initial design algorithm compare to the free wale lifting line algorithm, which takes into account much more physics into the solution (wake rotation effects, non-radial independence, 'root-correction', etc), Figure 3 shows the local design thrust coefficient (upper), design angles of attack (middle) and design lift coefficient (lower) as function of nondimensional radius computed with both a free wake method (full lines) and the inital design algorithm (circles). The results from the approximate BEM method is set up to have the same axial induction as the free wake results. This is the reason for the good agreement between the design angles of attack, as seen in the middle graph. Despite the exact match in the axial induction factor, the local thrust values from the approximate method does not match well. As a side note it is mentioned that the agreement in local power coefficient is equally bad. Turning now to the lower graph, we see that the agreement between the design lifts for the two methods are slightly less off than was the case for the local thrust coefficient. If the uncertainties for computing the airfoil coefficients on thick airfoils are taken into account (and the lack of applicable), it is concluded that the approximate design algorithm gives design-point results (corresponding values of angle of attack and lift coefficient) that can be used for the initial designs of slatted inner sections. For accurate analysis of the forces, however, the accuracy is probably not so good as the free wake

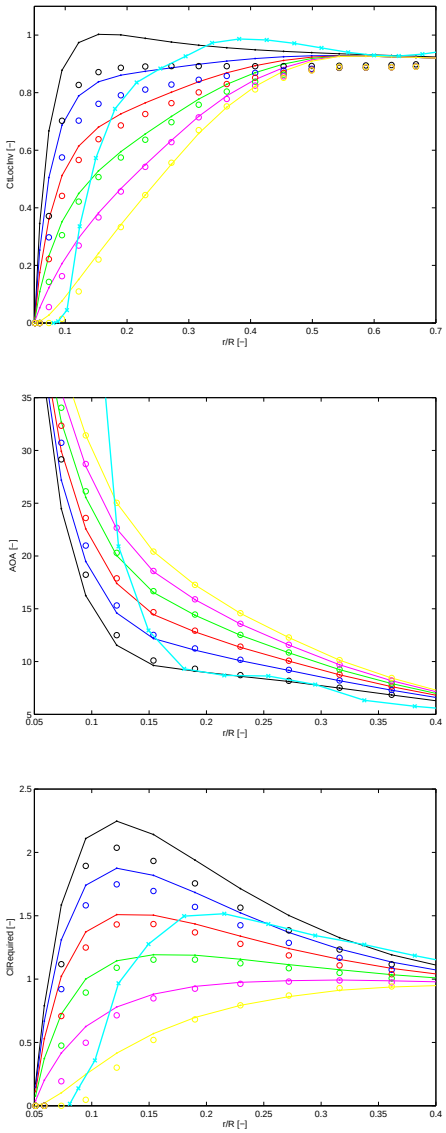

Figure 3: Local $C_{t,design}$ (upper), α_{design} (middle) and $C_{l,design}$ (lower), as functions of $\tilde{r}$. Full lines are free wake lifting line results and circles are approximate BEM results. The cyan curve corresponds to the solution of the 10RWT rotor with the basic setup at zero pitch at $\lambda = 8.06$.

lifting line method. For all cases it is seen that all values agree better for low loadings.

The results in the figure can now be used to determine designpoints for 2D slat optimizations of the inner sections on the rotor.

5.2 2D slat optimization

The present work aims at investigating the power production potential of adding slats to

the inner part of the 10MW reference wind turbine (RWT10). Two different design cases could be envisaged. 1: Design of a slat as an add-on to the "existing" RWT10 rotor. 2: Design of a main rotor-slat combination from scratch. As mentioned in the introduction, the second alternative could maximize the potential benefit available using the multiple element airfoils, but in order to restrict the design space, we consider here the first option, namely the design of a slat to fit an existing rotor design. The overall goal of the 2D optimization is to achieve a slat configuration which meets the target lift coefficients at a specified angle of attack (from the lifting line computations), while also providing a high maximum lift beyond the design point to provide enough lift reserve to tackle the large changes in angle of attack present on inner sections of wind turbine blades. Based on the results shown above, it was chosen to design slats for the sections at $r/R = [0.10; 0.15; 0.20; 0.25]$, which has relative thicknesses of $t/c = [0.90; 0.74; 0.56; 0.46]$. In order for the target lift from the lifting line solution to be met, it was chosen that the relative chordlengths of the slats should be $c_{slat}/c_{main} = [0.5; 0.5; 0.4; 0.3]$.

As described by Fuglsang and Bak in [20] the addition of gurney flaps to the root part of wind turbine blades is an attractive option because the performance of the thick airfoils can be boosted this way. Therefore, the two innermost very thick airfoils was fitted with gurney flaps to ensure a better performance, and thereby better speed-up at the location of the slat position, which in turn results in an increased performance of the slat.

The slatted airfoil sections resulting from the 2D aerodynamic optimization are shown in Figure 4 and examples of flowfield behavior in terms of u-velocity contours (upper) and pressure contours (lower) for the $r/R = 0.15$ profile for angles of attack $\alpha = 16^0$ (left) and $\alpha = 20^0$ (right) are shown in Figure 5. It is seen that it is the slat airfoil that carries most of the load, and that in the case of $\alpha = 20^0$, there exist a jet from the slit between the slat and the main airfoil, which moves over the suction side of the main airfoil, even though the flow behind it is fully stalled (close to zero velocity in its wake). This phenomenon was also observed in the wind tunnel by Zahle et.al. [15, 16].

Figure 6 show the integral airfoil force coefficients of the slatted airfoils in full lines, and

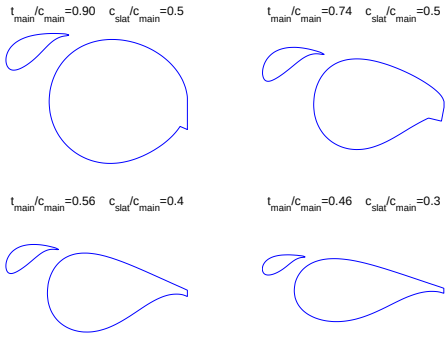

Figure 4: Geometry of the slatted sections at $\tilde{r} = 0.10$ (upper left), $\tilde{r} = 0.15$ (upper right), $\tilde{r} = 0.20$ (lower left) and $\tilde{r} = 0.25$ (lower right).

the corresponding force coefficients of the unslatted main airfoils in dashed lines. It is seen that the slats drastically increase the performance of the thick airfoil sections, both concerning magnitude of the lift as well as lift to drag ratios. Both these effects will have a positive effect on the power production.

5.3 Evaluation of power production increase

The power production increase will be evaluated using both using the power coefficient in the design point and the annual energy production. However, before proceeding to the evaluation, a discussion on the effects of rotational augmentation of the profile coefficients, or stall delay, is in order.

Findings from earlier studies [2, 7–9] show that as long as stall is avoided, the lifting-line free wake code combined with uncorrected 2D airfoil coefficients give results in good agreement with the CFD results. This indicates that as long as stalling conditions are avoided in the design, 2D data should be able to describe the aerodynamics well all the way in on the rotor without having to be 3D stall delay corrected. In the present case, with main airfoils having very high thicknesses, stall cannot be avoided on the main airfoil, so airfoil data from 2D simulations should probably be stall corrected. The problem here is that there exist no models that would take into account the physics of the multiple element airfoils correctly when doing the stall delay correction. The flow on the slat airfoil, which for the very thick main airfoil configurations are responsible for almost all lift generation, is designed to have a very limited stall

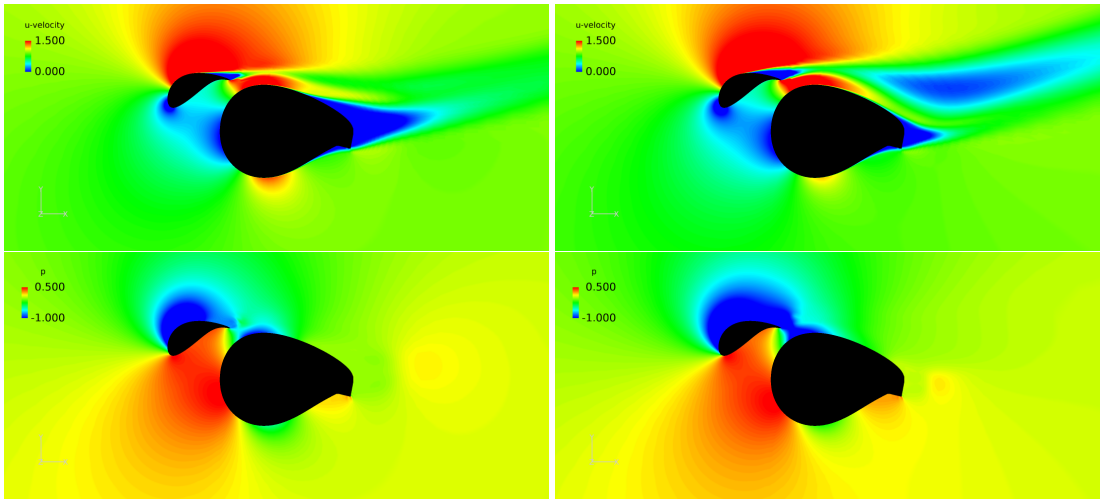

Figure 5: Examples of u-velocity- (upper) and pressure-contours (lower) of the main airfoil profile for angles of attack $\alpha = 16^0$ (left) and $\alpha = 20^0$ (right). The relative rotor radius for this example is $\tilde{r} = 0.15$, the relative airfoil thickness is $t/c = 0.74$ and the slat chordlength is $c_{slat}/c = 0.5$.

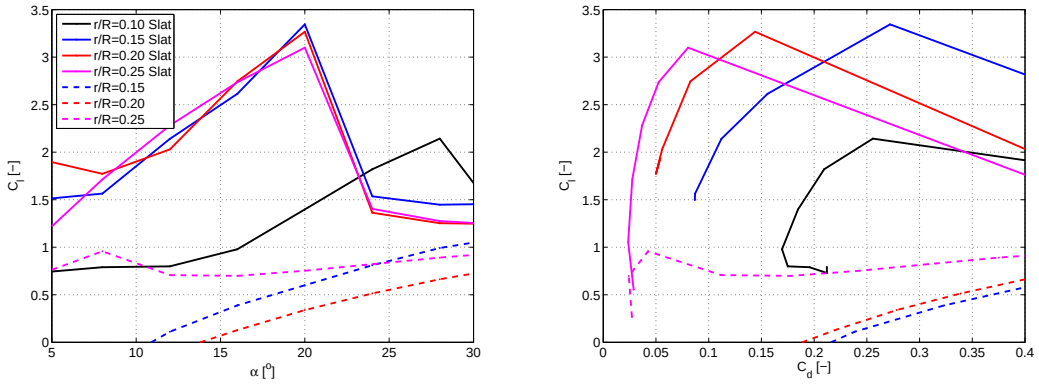

Figure 6: 2D CFD results of the optimized sections. C_l versus α (left) and C_l versus C_d for the slatted configurations (full lines) and for the main airfoils only (dashed lines). The length used for nondimensionalization of the forces are the main chordlengths.

at the operation point. Therefore, based on the earlier findings, it is not expected that this part of the total forces need stall corrections even though this might be needed for the main airfoils. Since, however, the effect of the slat depends on the loading/situation of the main airfoil, it is not unlikely that the loading on the slat airfoil will to some extent also be influenced by the stall corrections through the main airfoil behavior as a second order effect. Since both of these effects would lead to a higher lift, it is probably safe to state that the 2D polars for the slatted sections will be a conservative estimate for at least the lift in the real 3D case. The results in Tables 1 and 2 show the integral performance of the rotor (C_T and C_P) at the design point evaluated with the free wake model and the BEM model, respectively. The rotor aerodynamic models are run with three sets of airfoil data: the baseline stall delay corrected dataset ([5]), a dataset where the performance of the sections at the locations where the slats are located are predicted using 2D CFD data without stall delay modelling added, and lastly a slatted dataset from 2D CFD which is also not stall corrected. With the previous discussion on stall delay corrections in mind, it is seen that the power production performance of the rotor is increased significantly by addition of the slats. Exactly how much, on the other hand is hard to determine du to the uncertainty of the stall delay issue. To outline this issue

Case	C_P	C_T	$(C_P - C_{P,ref})/C_{P,ref}$	$(C_T - C_{T,ref})/C_{T,ref}$
Orig (ref)	0.486	0.864	-	-
2D CFD polars $r/R < 0.3$	0.463	0.832	-4.9%	-3.7%
Slat	0.497	0.872	+2.2%	+1.0%

Table 1: Integral performance at design point: $\lambda = 8.06$ and zero pitch. Free Wake Lifting Line results.

Case	C_P	C_T	$(C_P - C_{P,ref})/C_{P,ref}$	$(C_T - C_{T,ref})/C_{T,ref}$
Orig (ref)	0.490	0.868	-	-
2D CFD polars $r/R < 0.3$	0.470	0.838	-4.1%	-3.5%
Slat	0.499	0.876	+2.0%	+1.0%

Table 2: Integral performance at design point: $\lambda = 8.06$ and zero pitch. BEM results.

it is seen that the difference in power production between the reference case and the non-stall-delay-corrected case is above 4%. Maybe half of this increase should have to be added to the slatted case to get the true production increase. This is, however, merely speculations that would have to be confirmed for instance using 3D CFD. The results in Tables 1 and 2 further show that there is a quite good agreement on C_T and C_P as determined using the two different prediction tools despite the big difference in the level of physics that is considered in the models.

In order to evaluate the behavior of the slatted rotor in operation points other than the design point, Figure 7 show the relative increase in C_P and C_T compared to the baseline case for different tip speed ratios at zero pitch angle. It is seen that the performance increase

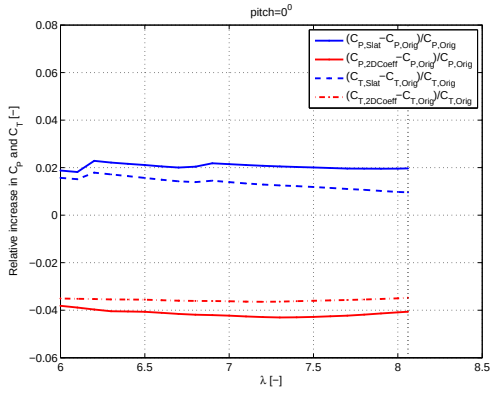

Figure 7: Off-design performance shown as relative increases in C_P and C_T compared to the baseline case.

is almost invariant of the tip speed ratio for the considered range. The results which the figure is based on is converted to power curve s

$\mid V_\infty \mid$	6 m/s	7 m/s	8 m/s	9 m/s
2D pol.	-3.1%	-2.5%	-2.1%	-1.8%
Slat	+1.4%	+1.2%	+1.0%	+0.8%

Table 3: Increase in annual energy production compared to (the stall delay corrected) reference case, BEM results. Weibull wind distributions with shape factor 2.

using the tip radius $R = 89.166\ m$, the maximum rotational speed of $\Omega_{max} = 0.8972\ 1/s$, a density of $\rho = 1.225\ kg/m^3$, a rated power of $P_{rated,mech} = 10^7\ W$ and a pitch setting of zero all the way to rated power. This way the effect on Annual Energy Production (AEP) can be assessed. The results from this study is shown in Table 3 As seen from the table the estimated increase in AEP is significant, but as mentioned above, the issues linked to stall delay corrections mean that the AEP increases are likely to be conservative estimates for the possible AEP gains.

6 Conclusion and Further Work

The present paper have

- Described a new CFD based tool for optimization of slats for thick airfoils
- Described the main mechanisms responsible for power production on a rotor in a simple way
- Described a simplified theory to aid in the design of slatted rotors
- Found that the power production potential by fitting slats on the inner part of design iteration 1 of the (quite heavily loaded)

10MW reference turbine is likely to be more than 1% AEP

- Stated that the beneficial effects of using slats may be larger if the slats and the main rotor blade are designed simultaneously
- Found that further work is needed to determine the AEP increase more accurately due to uncertainties in rotational effects/stall-delay
- Suggested that 3D CFD should be used to investigate a rotor with slats on to dig into these interesting issues

Acknowledgements

It is gratefully acknowledged that this work was partly funded by the Danish Energy Agency by the EUDP2010-I Light Rotor project. Furthermore, any work of this character would not have been possible without the patience of our loving wives and girlfriends.

References

[1] Madsen, H.Aa. *Two modifications of the BEM method based on validation with results of actuator disc results* In Research in Aeroelasticity EFP-2006. RisøReport 1611. 2006

[2] Johansen, J., Madsen, H, Aa., Gaunaa, M. and Bak C. *Design of a wind turbine rotor for maximum aerodynamic efficiency* Wind Energy, Vol. 12, 2009, p 261-273.

[3] Gaunaa, M., Sørensen, N. N. and Bak, C. *Thick Airfoils & High Lift* Chapter in: Research in Aeroelasticity, EFP-2007-II. Ed. Thomas Buhl. Risø-R-1698(EN). 2009.

[4] Gaunaa, M. & Sørensen, N. N. *Thick multiple element airfoils for use on the inner part of wind turbine rotors* In The Science of Making Torque from Wind, Crete, Greece, June 2010.

[5] Christian Bak, Robert Bitsche, Anders Yde, Taeseong Kim, Morten Hansen, Frederik Zahle, Mac Gaunaa, Jakob Wedel Heinen, Tim Behrens. *Light Rotor: The 10MW reference wind turbine* EWEA conference, Copenhagen, Denmark, 2012. Extended abstract submitted.

[6] Larsen, T. J. *How 2 HAWC2, the user's manual*. Technical Report Ris-R-1597 (ver. 3-7)(EN), Risø National Laboratory, DTU, Roskilde, Denmark, January 2009.

[7] Gaunaa, M & Johansen, J. *Can CP be Increased by the Use of Winglets? – or – A Theoretical and Numerical Investigation of the Maximum Aerodynamic Efficiency of Wind Turbine Rotors with Winglets*, 46th AIAA Aerospace Sciences Meeting and Exhibit, 7-10 January 2008, Reno, Nevada.

[8] Gaunaa M., Rethore P.-E. & Sørensen N.N. *Internal report: Efp07-ii 33033-0243, Design og optimering af vingetipper for vindmøller, risø contribution to final report*. Technical report, DTU, 2011.

[9] Mac Gaunaa, Pierre-Elouan Réthoré, Niels N. Sørensen and Mads Døssing *A computationally efficient algorithm for the aerodynamic response of non-straight blades*. EWEA conference 2011.

[10] Sørensen, N.N., *HypGrid2D, a 2-D mesh generator.* Technical report, Risø-R-1035(EN), Risø National Laboratory, 1998.

[11] Michelsen J.A. *Basis3D - a Platform for Development of Multiblock PDE Solvers.* Technical Report AFM 92-05, Technical University of Denmark, 1992

[12] Michelsen J.A. *Block structured Multigrid solution of 2D and 3D elliptic PDE's.* Technical Report AFM 94-06, Technical University of Denmark, 1994

[13] Sørensen N.N. *General Purpose Flow Solver Applied to Flow over Hills.* Risø-R-827-(EN), Risø National Laboratory, Roskilde, Denmark, June 1995

[14] Sørensen, N. N. *Prediction of Multi Element Airfoils With the EllipSys Code* Chapter in: Research in Aeroelasticity, EFP-2007-II. Ed. Thomas Buhl. Risø-R-1698(EN). 2009.

[15] Frederik Zahle, Mac Gaunaa, Niels N. Sørensen & Christian Bak *Design and Wind Tunnel Testing of a Thick, Multi-Element High-Lift Airfoil.* EWEA conference 2012. Extended abstract submitted.

[16] Frederik Zahle, Mac Gaunaa, Niels N. Sørensen & Christian Bak *Design of a Thick, Flatback, Multi-Element High-Lift*

Airfoil. Chapter in Aeroelastic Optimization of MW Wind Turbines, Risø-DTU, Technical Report, Risø-R-1803(EN), December 2011.

[17] OpenMdao webpage: *http://openmdao.org* Accessed MArch 9th 2012.

[18] Døssing, Mads*Optimization of wind turbine rotors - using advanced aerodynamic and aeroelastic models and numerical optimization* PhD thesis, Risø-PhD-69(EN). 2011. Wind Energy Division, Risø National Laboratory, DTU.

[19] Hansen, M.O.L. *Aerodynamics of Wind Turbines —Rotors, Loads and Structures* Textbook. James & James (Science Publishers) Ltd., 2000.

[20] Fuglsang, P. & Bak, C. *Development of the Risø Wind Turbine Airfoils* Wind Energy, Vol. 7, 2004, p.145-162.